Chapter 19

Numerical Simulation of Droplet Dynamics in Membrane Emulsification Systems

Manabendra Pathak

Additional information is available at the end of the chapter

http://dx.doi.org/10.5772/50180

1. Introduction

An emulsion is a two-phase liquid system of two immiscible liquids, where the liquid with lower mass fraction is dispersed in form of small droplets in other surrounding liquid of higher mass fraction. Emulsions are widely used to produce sol–gel, drugs, synthetic materials, and food products. Based on the size of droplet, emulsions can be classified as micro and macro emulsion. Karbstein and Schubert, (1995) have made a limiting droplet size of 0.1 μm, below which the emulsion is termed as micro emulsion and above that size the emulsion is termed as macro emulsion. Size and size distribution of droplets play important roles in the stability of emulsion. There are also other factors such as sedimentation, skimming, droplet aggregation and coalescence, which may affect the stability of the droplets. Thus for making a stable emulsion it is necessary to convert the dispersed phase into tiny droplets and stabilize them against coalescence. Some amount of energy is required in the process to break the dispersed phase into droplets. The amount of energy put in the dispersing phase also controls the resulting droplet size. The stability of newly formed droplets depends on how fast the used emulsifiers are able to occupy the newly created interfaces and how well they stabilize them. The common devices used to produce emulsions are rotor-stator-systems, stirrers and high-pressure homogenizers. During last two decades, new technologies of making emulsion have been developed. Compared to conventional method of emulsification such as rotor-stator method, these new techniques of emulsification have several advantages such as low energy consumption, controllable droplet size with proper distribution and easy scalability. These new methods are based on the microdroplet formation in micrometer sized channels. Three such new methods are T-junction emulsification, flow focusing emulsification, and membrane emulsification. In all these methods, controllable droplet formations are achieved by properly maintaining the combination of continuous and dispersed phase flow rate.

In membrane emulsification process, micro or macro porous membranes are used to generate droplets by pressing the dispersed phase through the porous matrix of the

membrane towards the continuous phase. At the interface, the dispersed phase forms droplets near the region of pores openings and detached by the cross-flowing continuous phase. Sometimes surfactants are used to stabilize the droplets. Compared to the conventional method, membrane emulsification process requires a lower energy input (10^5 – 10^6 J/m^3) to generate micro-sized droplets (Schubert and Behrend, 2003). Since small droplets are directly formed at the micro-pores of a membrane, rather than by disruption in zones of high energy density, smaller amount of stress is required in the process compared to the conventional method. The main disadvantage of the process is the requirement of longer production time compared to the conventional processes because of the slow rate at which the dispersed phase flows through the membrane (Joscelyne and Trägårdh, 1991, 2000). The longer production time can be reduced by increasing the flow rate of dispersed phase fluid. With the increase in dispersed phase flow rate, the droplet diameter increases first than decreases and the process shifts towards jetting phenomenon (Pathak, 2011). Thus there should be an optimum dispersed phase flux for optimum production time and droplet size in a membrane emulsification system.

The schematic diagram of a cross-flow membrane emulsification has been shown in Fig. 1. Some commonly used membranes are tubular micro-porous glass (MPG) and shirasu porous glass (SPG) membrane. Some metallic oxides such as ceramic α-Al_2O_3 or α-Al_2O_3 coated with titainia oxide or zirconia oxide are also used as membrane. These membranes contain cylindrical, interconnected, uniform micro-pores having pore sizes, typically ranging about 0.05–14 μm. In membrane emulsification system, the time of droplets formation, size and stability of droplets are three important parameters which control the emulsification system. Thus understanding the droplet dynamics in detail may enable to explore the possibilities and limits of membrane emulsification for various applications.

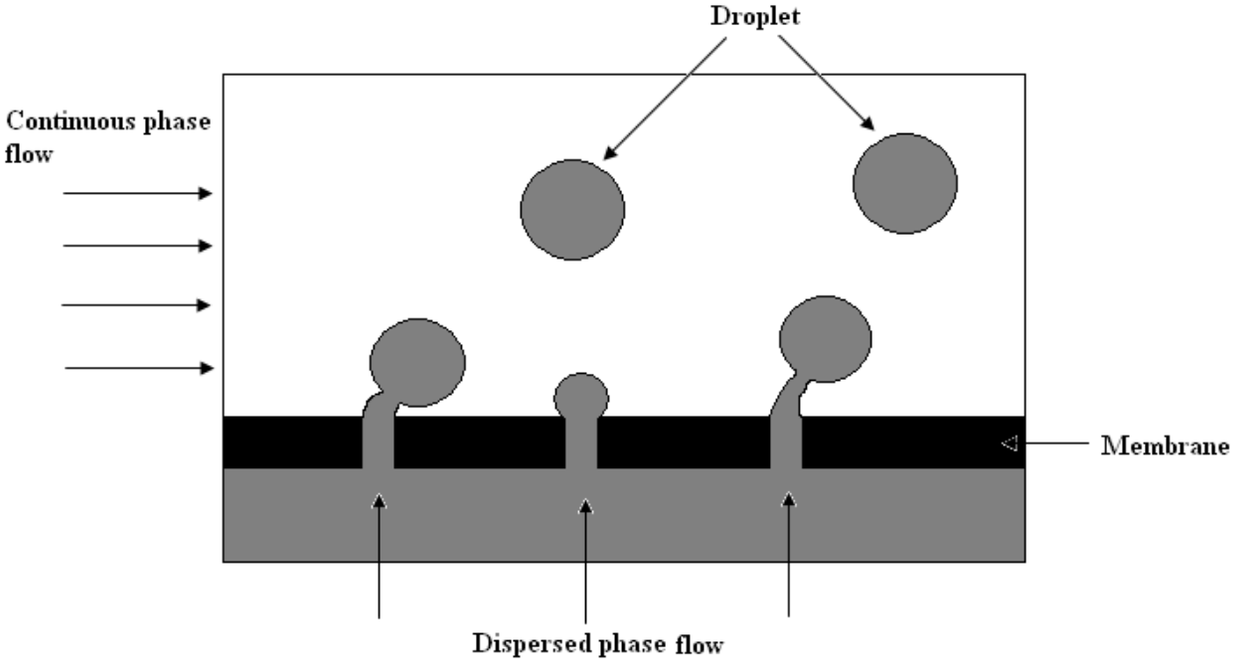

Figure 1. Schematic diagram of a cross-flow membrane emulsification process

In membrane emulsification process, the size distribution of pores and their relative spatial distribution in the membrane surface control the production of mono-disperse emulsions. The growth and detachment of the droplet i.e. droplet dynamics in membrane emulsification depends on several parameters. Luca et al., (2004) has classified them into three broad categories.

i. **Operating parameters:** cross-flow velocity, transmembrane pressure and disperse phase flux;
ii. **Membrane parameters:** pore size, active pores, distance between the pores, membrane hydrophobicity/hydrophilicity;
iii. **Phase parameters:** interfacial tension, viscosity and density of the processed phases.

Based on these parameters, the size of the droplet in membrane emulsification system depends upon the pore diameter and the dependence of the droplet diameter on pore diameter can be expressed as:

$$D_p = x\, D_0 \tag{1}$$

where D_p is the droplet diameter and D_0 is the pore diameter. Katoh et al., (1996) experimentally observed the value of x in the range of 2 to 12. The major factors affecting the value of x are: (i) the shear rates of continuous cross-flow fluid (ii) the dynamic interfacial tension, γ; and (iii) the disperse phase flux (J_d). Other parameters those implicitly control the value of x are: the average velocity of the continuous phase flow $\langle u_c \rangle$, the viscosities of the disperse phase and the continuous phases (μ_d and μ_c) the density of the continuous phase (ρ_c) the thermodynamic temperature, (T), the transmembrane pressure (P_m). The viscosity and dynamic surface tension depend upon temperature and that way temperature can influence the emulsification process.

Cross-flow velocity of continuous phase imparts drag force on the growing droplet for which the droplet detaches at the pore. With the increase in cross-flow velocity, the droplet diameter decreases. The dispersed phase flow rate or velocity influences the droplet dynamics via the inertial force competing with other forces such as drag and surface tension force. The difference between the pressure of dispersed phase in the dispersed phase channel and the average pressure of the continuous phase in the main channel is termed as transmembrane pressure.

$$\Delta p_m = p_d - \overline{p_c} \tag{2}$$

The average pressure of the continuous phase is defined as:

$$\overline{p_c} = (p_{c,in} + p_{c,out})/2 \tag{3}$$

where $p_{c,in}$ and $p_{c,out}$ are the pressure of continuous phase at the inlet and outlet of the main channel. Total transmembrane pressure consists of two parts: one is the capillary pressure (p_γ) and other is the effective transmembrane pressure (p_{eff}) or drag pressure inside the pore. Due to curvature of the droplet and dynamic interfacial tension, a small amount of pressure is required to inflate the droplet. This pressure is the capillary pressure. The capillary

pressure is maximum at the starting of formation of the droplet at the pore and it decrease as the droplet grows. The capillary pressure becomes the minimum at the detachment time of the droplet. The effective or drag pressure part is responsible for the flow rate of dispersed phase. The effective pressure determines the throughput and thus the productivity of the membrane emulsification system. The transmembrane pressure controls the size of the droplet formed in membrane emulsification process. With the increase in transmembrane pressure, several researchers (Katoh et al, 1996; Peng and Williams, 1998; Schröder and Schubert, 1999) have observed the increase in droplet diameter while others (Abrahamse et al., 2002; Vladisavljevic and Schubert, 2003; Vladisavljevic et al., 2004) have observed the decrease in droplet diameter. The variation in droplet diameter with transmembrane pressure results the wide range of droplet size distribution (Abrahamse et al., 2002; Vladisavljevic et al., 2004). The wide range of droplet size also is affected by the steric hindrance between droplets or by the membrane being wetted by the dispersed phase, causing coalescence on the membrane.

The design and pore distribution of the membrane are important factors controlling the droplet dynamics in membrane emulsification. Due to presence of multi-pore and multi-droplet formation, there is a change in hydrodynamic effects caused by neighboring droplet and interactions between the droplets. The separation distance between the pores controls those hydrodynamic effects. If the separation distance of pores in the flow direction is small, the continuous phase velocity decreases and the boundary layer thickness increases as the flow approaches consecutive rows after crossing the first row. These would lead to an increase in the size of the droplets. With the increase in droplet size, there would be a caution of stability loss and coalescence of the droplets. For high efficiency of the emulsification process, narrow droplet size distribution and higher dispersed phase velocity is required. However, with the increase in dispersed phase flow rate, the droplet formation phenomenon shifts towards jetting (Pathak, 2011) and this requires a greater distance between the pores in the direction of the cross-flowing continuous phase in order to prevent drops from colliding and coalescing. In several experimental studies (Sugiura et al., 2002; Kobayashi et al, 2003, 2006) the droplet size distribution has been observed narrow up to a specific velocity of the dispersed phase, above which the diameter of the droplet distribution has been increased. Timgren et al. (2009) have investigated the effects of pore size distribution on hydrodynamic effects of droplet size and distribution. They observed that for small pore separation distance and with a low dispersed phase velocity the drop formation process was uniform, resulting an emulsion with a narrow drop size distribution. For shortest pore separation distance, with the increase in dispersed phase velocity, they observed the formation of poly dispersed emulsion, whereas pore separations of 15 and 20 times the pore diameter gave nearly mono dispersed emulsions.

The wetting behavior of membrane surface also controls the droplet growth. The wetting behavior of a membrane is represented by the static contact angle between the two liquid phases and the solid boundary. The static contact angle between the two phases and walls controls the evolution of the dispersed phase inside the micro-pore and in the continuous phase flow channel. If the angle is less than 90^o the wall is said to be wetting and if it is greater than 90^o, the wall is called the non-wetting.

Among different properties of the phase, surface tension controls the droplet dynamics in a greater way than any other properties. Surface tension force holds the droplet and offers the resistance against any deformation. The viscosities of both the phases have also effect on the droplet deformation. The drag force imparted by the continuous phase on the droplet depends upon the viscosity ratio of dispersed phase and continuous phase. For fixed flow rate of continuous phase the drag force increases with the increase in viscosity ratio up to some extent. After that value, the drag force becomes independent of the viscosity ratio. The densities of both phases enter into the droplet dynamics through the buoyancy or gravity force. In micro- or nano-fluidics flow the value of gravity force is very small and it can be neglected without loss of much accuracy.

1.1. Different forces acting in membrane emulsification.

All the parameters discussed in above control the droplet dynamics in membrane emulsification process with different magnitudes and output of the process can be analyzed on the basis of these operating parameters. Besides the individual effects, many of these parameters exhibit coupling effects. Different types of hydrodynamic forces act in the emulsification process. The droplet growth and deformation in membrane emulsification can be explained from the action of these and the final droplet size is a result of the interaction of these forces.

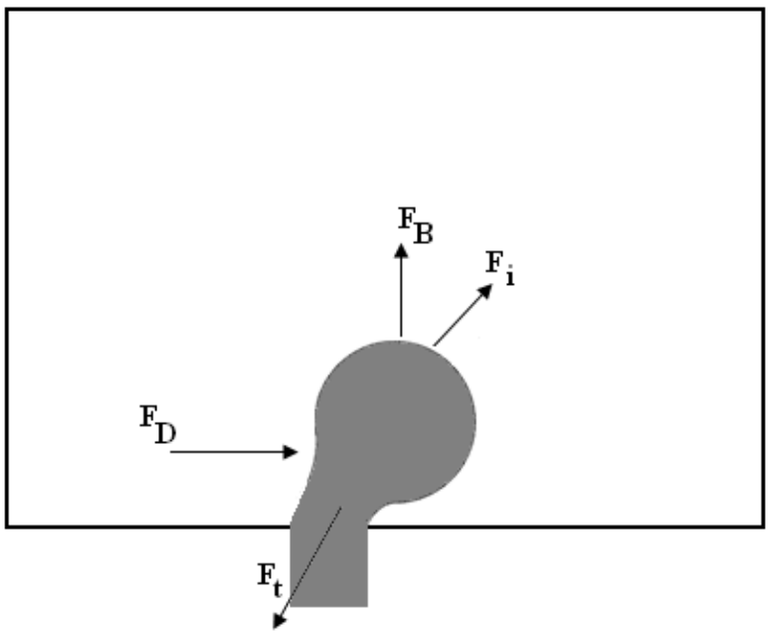

Figure 2. Different forces acting on the emulsification system

The major forces that act in the process are: drag force imparted by the flowing continuous phase, the interfacial tension force, the inertial force of the dispersed phase and the buoyancy or gravitational force. Different forces acting in the droplet formation process are shown in Fig. 2. Among these forces, interfacial tension force is the attaching force and other are detaching force. The droplet is detached from the pore when the detaching forces overcome the attaching force.

These four forces can be approximated as follows:

Drag force:

$$F_D = \frac{1}{2} C_d \rho_{cp} (v^* - v_{dp})^2 (\pi D_P^2 / 4) \tag{4}$$

Surface tension force:

$$F_t = \pi \sigma D_p \tag{5}$$

Inertial force of dispersed phase:

$$F_i = \frac{\pi \rho_{dp} D_0^2 v_{dp}^2}{4} \tag{6}$$

Buoyancy force:

$$F_B = \rho_c g V_{dr} - p_c A_n \tag{7}$$

In above v_{dp} is the velocity of dispersed phase ($v_{dp} = v_o$), v^* is the local continuous phase velocity at the centre of the drop, D_p is the diameter of the drop, D_0 is the pore diameter and V_{dr} is the droplet volume. The local continuous phase velocity is given by:

$$v^* = 2u_{cp} \left[1 - \left(\frac{D_h - D_p}{D_h} \right)^2 \right] \tag{8}$$

where u_{cp} is the average velocity of the continuous phase in the channel. D_h is the hydraulic diameter given by:

$$D_h = 2bh / (b + h) \tag{9}$$

where b and h are the width and height of the continuous phase channel respectively. The drag coefficient C_d depends upon the Reynolds number of the droplet (Re_p) and the viscosity ratio λ (μ_{dp} / μ_{cp}) . The drop Reynolds number is defined as

$$Re_p = \frac{\rho_{dp} \left| v^* - v_{dp} \right| D_p}{\mu_{dp}} \tag{10}$$

Out of these forces, the only attaching force is the surface tension force and remaining forces, drag and inertial and buoyancy force are detaching forces. Neglecting the buoyancy or gravity force, the balance of forces at the moment of droplet detachment can be written as

$$\frac{1}{2} C_d \rho_{cp} (v^* - v_{dp})^2 (\pi D_P^2 / 4) + \frac{\pi \rho_{dp} D_0^2 v_{dp}^2}{4} = \pi \sigma D_p \tag{11}$$

For low value of *We* number, the value of inertial force (F_i) is very low. In that situation the diameter of the drop can be approximated as

$$D_p \propto \frac{\sigma}{(C_d \rho_{cp})(v^* - v_{dp})^2} \tag{12}$$

Thus analytically, droplet diameter increases with the increase in surface tension value.

1.2. Numerical simulation of droplet dynamics

Droplet formation and deformation have been studied for a long time due to complexity with the problem and practical utilities of the phenomenon. Droplet formation in a two-phase flow system possesses a rich dynamics with the involvement of several parameters such as average velocity of the liquids, their viscosities, densities, surface tension, surface chemistry and the flow geometry. Droplets formation results the creation of new surfaces which enhance the heat and mass transfer between the phases. Due to enhanced heat and mass transfer, the process has been used for wide ranges of phase-contact applications. Particularly the droplet formation in micro or nano size has received significant attention during last several years. Due to miniature size, the fabrication of experimental facility is expensive and reliable experimentation of microfluidic is very intricate. Hence the viable alternate is the numerical tools for investigating the problems. With the development of high speed computer and advanced algorithm, numerical modeling and simulation have become an essential part in the design and development of numerous engineering systems. Numerical simulations of droplet dynamics i.e. the investigations of two-phase flow in micro scale have been extensively undertaken during last several years. Various types of numerical techniques have been developed to solve the governing equations of the two-phase flow.

1.3. Different numerical methods

In numerical simulation of droplet dynamics or as a whole in the simulation of two-phase flow, there are several challenges which need to be carefully tackled to obtain reliable results. The main challenge is capturing the moving interface of the two phases accurately, which is not known priory. The accurate tracking of the interface and investigation of two-phase flow topology should be the essentiality of a good numerical method. There are several numerical methods based on interface kinematics to track the interface in free surface flows. Among them are: volume of fluid methods, front tracking methods, level set methods, phase field formulations, continuum advection schemes, boundary integral methods, particle-based methods, and moving mesh methods.

Volume of fluid method (VOF), earlier known as the volume tracking method, were originally developed by Nichols and Hirt (1975), Noh and Woodward (1976) and further extended by Hirt and Nichols (1981). Since then, the method has been extensively used and significantly improved over the years (Rudman,1997; Rider and Kothe,1998). The VOF

method is based on the conservation of the volume fraction function F with respect to time and space, expressed as

$$\frac{\partial F}{\partial t} + (v.\nabla)F = 0 \tag{13}$$

In VOF method, the computational grid is kept fixed and the interface between the two fluids is tracked within each cell through which it passes. In a computational grid cell, the interface can be effectively represented by line of the slope. To reconstruct the interface, the piecewise linear interpolation calculation (PLIC) method developed by Youngs (1982) is used in the computation. The interfacial surface forces are incorporated as body forces per unit volume in the Navier-Stokes equations; hence no extra boundary condition is required across the interface.

The basic working principle of front tracking method is based on the marker and cell (MAC) formulation (Harlow and Welch, 1966; Daly, 1967). The interface is represented discretely by Lagrangian markers connected to form a front which lies within and moves through a stationary Eulerian mesh. As the front moves and deforms, interface points are added, deleted, and reconnected as necessary. Further details of the method may be found in (Glimm et al., 1985; Churn et al., 1986; Tryggvason et al., 1998).

Level set methods have been developed by Osher and Sethian (1988). This method can compute the geometrical properties of highly complicated interface without explicitly tracking the interface. The basic principle of the level set method is to embed the propagating interface Γ(t) as the zero level set of a higher dimensional function ϕ , defined as ϕ (x, t =0) = ±d, where d is the distance from x to Γ (t = 0). The function is chosen to be positive (negative) if x is outside (inside) the initial position of the interface Γ (t = 0) = ϕ (x, t =0)=0. Afterwards a dynamical equation for ϕ (x, t =0) that contains the embedded motion for $\Gamma(t)$ as the level set ϕ =0 can be derived similarly as in the volume of fluid conservation equation (13)

In phase field method, interfacial forces are modeled as continuum forces by smoothing interface discontinuities and forces over thin but numerically resolvable layers. This smoothing allows conventional numerical approximations of interface kinematics on fixed grids. The method has been used for investigating the problems governed by Navier-Stokes equations (Antanovskii, 1995; Jacqumin, 1996).

Boundary integral methods are designed to track the interface explicitly, as in front tracking methods, although the flow solution in the entire domain is deduced solely from information possessed by discrete points along the interface. The advantage of these methods is the reduction of the flow problem by one dimension involving quantities of the interface only.

Particle-based methods use discrete "particles" to represent macroscopic fluid parcels. Here, Lagrangian coordinates are used to solve the Navier-Stokes equations on "particles" having properties such as mass, momentum, and energy. The nonlinear convection term is modeled simply as particle motion and by knowing the identity and position of each particle,

material interfaces are automatically tracked. By using particle motion to approximate the convection terms, numerical diffusion across interfaces (where particles change identity) is virtually zero; hence interface widths are well defined.

In moving mesh methods, the position history of discrete point's x_i lying on the interface is tracked for all time by integrating the evolution equation, forward in time.

$$\frac{dx_i}{dt} = v_i \tag{14}$$

A moving mesh is Lagrangian if every point is moved, and mixed (Lagrangian-Eulerian) if grid points in a subset of the domain are moved. Mixed methods are used for mold filling simulations, where the mold computational domain can be held stationary and the molten liquid is followed with a Lagrangian mesh.

Besides these individual methods, there are some combined method such as coupled level set and volume of fluid method. This method has been developed to tackle the inefficiency of VOF method in calculating complex geometrical properties and problem of mass imbalance of level set method. In the coupled method, the LS function is used only to compute the geometric properties (normal and curvature) at the interface while the void fraction is calculated using the VOF approach. Ohta et al. (2007) and Sussman et al. (2007) developed a novel coupled LS-VOF method to determine the sharp interface for incompressible, immiscible two-phase flows for large value of density ratio.

1.4. Issues of numerical simulation

Numerical investigation of active droplet formation is reasonably complex as it is potentially a multi-physics problem governed by a large number of partial differential equations (PDEs). Numerical simulation of droplet dynamics in membrane emulsion process requires accurate capturing of the evolving liquid–liquid interfaces. This gives sufficient challenge since the boundary between the two phases is not known priori and it is a part of the solution. In addition, the solution technique has to deal with different properties of both the phases such as density, viscosity, and velocity ratios. Numerical investigation of membrane emulsification process requires two main issues to be dealt with: one is permeation of the disperse phase through the membrane pores; the other is the mechanism of droplet detachment. Several earlier investigations have treated these issues separately; however both of them simultaneously contribute to droplet evolution and should be considered in the same framework. Both these issues have been considered in the present work. In the present work, numerical simulation of droplet dynamics in a membrane emulsification has been carried out considering multipore membrane. The hydrodynamic effects due to multipores and the effect of different operating parameters on the droplet dynamics have been investigated.

2. Problem description

The flow configuration of membrane emulsification considered in the present work has been shown in Fig. 3. Here the membrane emulsification process with two pores has been

considered. A uniform pore arrangement in the membrane surface has been considered and the simulation has been mode for a row of pores consisting of two pores. The dispersed phase liquid has been injected through cylindrical pores of 10 μm diameter and a length of 100 μm. The distance between the pores in cross-flow direction has been considered as 100 μm. The height of the rectangular channel through which the continuous phase flows has been considered as 150 μm (y-direction). The width of the computational domain has been considered as 150 μm (z-direction) and a length of 500 μm (x-direction) has been considered. Since the present computational domain is a small element of whole membrane emulsification process, symmetrical boundary conditions have been considered in both the sides of computational domain in z-direction. The fluid properties used in the present simulation are within the range of properties of o/w emulsion system. Simulations have been made for different values of the non-dimensional numbers and other flow properties as shown in Table 1.

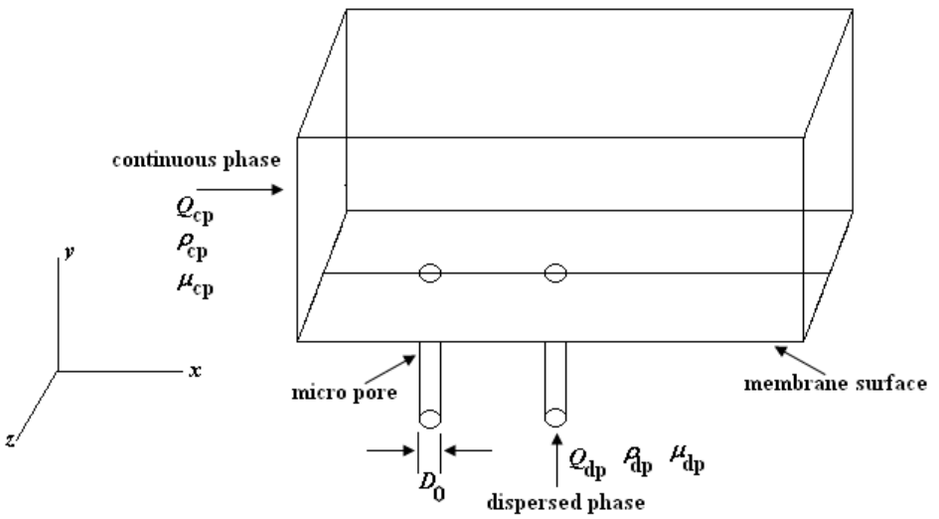

Figure 3. Schematic of computational domain

2.1. Governing equations

In the simulation of membrane emulsification system, both the phases have been considered incompressible, isothermal and laminar flow. The phase properties and the surface tension have been assumed to be constant throughout the flow domain. The conservation of mass on the whole domain (both the fluid phases and interface) leading to continuity equation is written as:

$$\frac{\partial \rho}{\partial t} + \nabla.(\rho V) = 0 \tag{15}$$

The momentum equation or unsteady Navier-Stokes equation is written as:

$$\rho\left(\frac{\partial V}{\partial t} + V.\nabla V\right) = -\nabla p + \rho g + \nabla.\left[\mu(\nabla V + \nabla V^T)\right] + f_S \tag{16}$$

In above f_S is the surface force, which includes surface tension force of the interface of the two fluids.

Parameters	Ranges
Diameter of pore	10 μm
Flow rate of continuous phase	0.27 and 0.54 liter/h
Flow rate of dispersed phase	0.0014 to 0.007 liter/h
Viscosity of continuous phase	0.001 Pa.s
Viscosity of dispersed phase	0.0036 to 0.014 Pa.s
Density of continuous phase	1000 kg/m^3
Density of dispersed phase	827 kg/m^3
Surface tension	0.0008 to 0.0024 N/m
Weber no (*We*)	0.0021 to 0.215
Capillary no (*Ca*)	0.0208 to 0.0625
Froude no (*Fr*)	6.37 to 637

Table 1. Values of physical properties used in the simulation

2.2. Interface tracking

Volume of fluid method (VOF) has been used for tracking the interface. In this method, the distribution of volume fraction is solved from its transport equation.

$$\frac{\partial F}{\partial t} + V.\nabla F = 0 \tag{17}$$

With the inclusion of volume fraction in the calculation, the volume averaged density and viscosity (ρ and μ) are defined as:

$$\rho = \rho_1 + F(\rho_2 - \rho_1) \tag{18}$$

$$\mu = \mu_1 + F(\mu_2 - \mu_1), \tag{19}$$

where subscript 1 and 2 denote the continuous and dispersed phase respectively. The surface force f_S appearing in momentum equation has been calculated using continuous surface force (CSF) model proposed by Brackbill et al. (1992) . It is defined as:

$$f_S = -\sigma\kappa\nabla F, \tag{20}$$

where σ and κ are the surface tension and surface curvature respectively. Surface curvature is calculated from:

$$\kappa = \nabla.\frac{\nabla F}{\left|\nabla F\right|}. \tag{21}$$

2.3. Boundary and initial conditions

Various types of boundary conditions have been used in the simulation of the membrane emulsification. A fully developed laminar duct flow has been considered at the inlet to the continuous phase channel and the flow has been assumed to be dominant along the stream direction thus: $u = u_{cp}$, v = 0, w = 0. At the inlet of continuous phase, the value of volume fraction has been set to zero (F = 0). At the inlets to the micro-pores, a velocity inlet type boundary condition has been used: $v = v_0$. The other components of the velocity have been put as u = 0, w = 0 and the value of volume fraction has been set to F = 1. Outflow boundary condition has been put at the outlet of the flow channel. Symmetry boundary conditions have been put at both sides of the computational domain. The top of the channel has been treated as walls where no-slip and impermeability boundary conditions have been set. At the starting of the computation, the whole flow domain has been assumed to be filled up with the continuous phase fluid. The static contact angle between the two phases and the wall influences the droplet growth in the dispersed and continuous phase channel. It has been observed that the effect of contact angle in the droplet formation is negligible when its value is greater than 165° (Sang et al., 2009). The value of static angle used in the present simulation has been set to 170°.

To reduce the number of dependable variables, the governing equations have been expressed in dimensionless form. The diameter of the pore (D_0) has been used as length scale and the average velocity (v_0) of the dispersed phase has been used as velocity scale for making non-dimensional form of the equation. The non-dimensional equations are:

$$\frac{\partial \rho^*}{\partial t^*} + \nabla.(\rho^* V^*) = 0 \tag{22}$$

$$\left(\frac{\partial V^*}{\partial t^*} + V^*.\nabla V^*\right) = -\nabla p^* + \frac{\rho^*}{Fr} + \frac{1}{\mathrm{Re}}\nabla.\left[(\nabla V^* + \nabla V^{*T})\right] + \frac{1}{We}.\ \nabla.\frac{\nabla F}{|\nabla F|} \tag{23}$$

In above starred quantities are non-dimensional parameters. The three non-dimensional numbers appeared in the problem are: Reynolds number (Re) , Weber number (We) and Froude number (Fr). They are defined as:

$$Re = \frac{\rho_{dp} v_0 D_0}{\mu_{dp}};\ We = \frac{\rho_{dp} v_0^2 D_0}{\sigma};\ Fr = \frac{v_0^2}{g D_0};$$

The Reynolds numbers (Re) is defined as the ratio of viscous force to the inertia force, Weber number (We) is defined as the ratio of inertia force relative to the surface tension force and Froude number (Fr) is defined as the ratio of inertia to gravity force. In the present work to incorporate the effect of the continuous phase fluid, the Capillary number has been introduced and is defined as:

$$Ca = \frac{\mu_{cp} u_{cp}}{\sigma} = \frac{RWe}{\lambda \mathrm{Re}}$$

where λ is the viscosity ratio ($\lambda = \mu_{dp} / \mu_{cp}$) and R is the velocity ratio ($R = u_{cp} / v_0$).

2.4. Numerical method

Commercial code Ansys Fluent (V12) based on finite volume method has been used in the simulation. The momentum and volume fraction transport equation have been discretized with 2nd order upwind scheme. The PISO (pressure implicit with splitting of operators) algorithm has been used for pressure correction. The VOF/CSF techniques have been used to track the fluid interface between the two immiscible fluids. A geometry reconstruction scheme has been used in the simulation to avoid the diffusion at the interface. The interface was reconstructed by the piecewise-linear interface calculation (PLIC) technique (Youngs, 1982). The unsteady term was treated with first-order implicit time stepping. Simulations were made with very small time steps (~10^{-7} s). The solutions have been assumed to be converged and therefore iterations have been terminated when the normalized sum of residual mass was less than 10^{-4} and variation of other variables in successive iteration was less than 10^{-2}. A non-uniform grid was used in the simulation where grids were clustered near the walls and the injection portion of the dispersed phase. The channel was decomposed into 12×10^5 numbers of control volumes and the pore with 12×10^3 after a grid independent study.

3. Results and discussions

In the present work, the dynamics of droplet formation in two pores of membrane emulsification has been investigated for different flow rates (velocities) of dispersed phase, continuous phase, surface tension and viscosity of the two phases. It is to be noted that In case of membrane emulsification process, the dispersed phase fluid gets more space to interact with the continuous phase fluid compared to the confined geometries in case of T-junction emulsification. Due to this the evolution of dispersed phase becomes different than the case of T-junction emulsion and the dependence of the process on different properties of both the phases also changes.

3.1. Growth and detachment of the droplets

In membrane emulsification system, the flow rate of dispersed phase controls the droplet dynamics via its inertial force competing with the drag force imparted by the continuous phase and interfacial tension force. In order to investigate the effect of dispersed phase flow rate, simulations have been made for different values of *We* number by changing the dispersed phase velocity i.e. inertial force and keeping the surface tension force fixed. Before discussing the effects of *We*, the growth and detachment of the droplet for a constant values of *We* (0.0086) and *Ca* (0.028) at different time levels have been shown in Fig. 4. It has been observed that both the droplet grow at their respective micro-pore and detached by the

continuous phase at the same location. As the first droplet is being detached and carried away by continuous phase fluid, the second droplet starts to grow at the pore and the repetition of droplets detachment takes place periodically with constant volume of droplet. Simulation has also revealed that the growth rate of the droplet at the downstream micro pore is different than the upstream micro pore and the droplet at that pore requires more detachment time. The presence of upstream droplet changes the hydrodynamic effects and reduces the viscous drag force of continuous phase on the downstream droplet. Due to reduction in drag force, the surface tension force can hold the droplet for longer time and detachment takes place lately. Due to this the droplet size is greater than the droplet formed at the upstream pore. Moreover due to low drag force of the continuous phase, the inertia force of dispersed phase has some effect in forming the necking of the droplet in the downstream pore. The diameter of the droplet after detachment has been found as 41.3 μm, which is about 4.13 times the pore diameter. This ratio is within the range of 1-12 observed by Katoh et al. (1996).

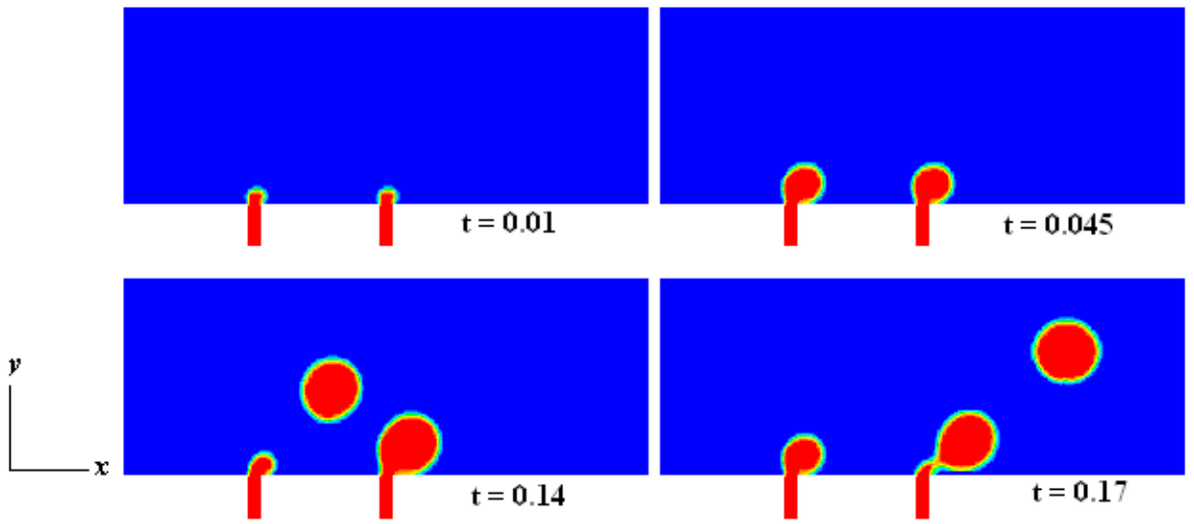

Figure 4. Growth and detachment of droplet at different time level, *We* = 0.0086, *Ca* = 0.0208

Thus the distance between the two pores should be at least five times the pore diameter for simultaneous growing of two spherical droplets without any hindrance from the neighboring pore. On the other hand the droplet deforms in the direction of flow of the continuous phase as shown in Fig. 4. Considering the deformation and growth of the droplet, it can be concluded that a distance of almost 10 times the pore diameter between the two pores in *x*-direction i.e. in cross-flow direction is needed to avoid contact, and thus avoid coalescence at two neighboring pores for this particular flow rate of dispersed phase and surface tension.

The investigation of droplet growth in transverse direction i.e. *z*-direction is important to design the pore distance in transverse direction. The growth of the droplet in a horizontal plane (*x*-*z*) at at y/D_0 = 25 μm has been shown in Fig. 5 at different time levels for *We* = 0.0086 and *Ca* = 0.0208. As the time progresses, the droplet at the first pore grows and deforms along the cross-flow fluid direction. Thus the distance between the two forming

droplets decreases. It has been observed that in the transverse (*z*-) direction the droplet remains almost spherical throughout the formation process; therefore, the distance between the pores in that direction can be fixed at seven times the pore diameter.

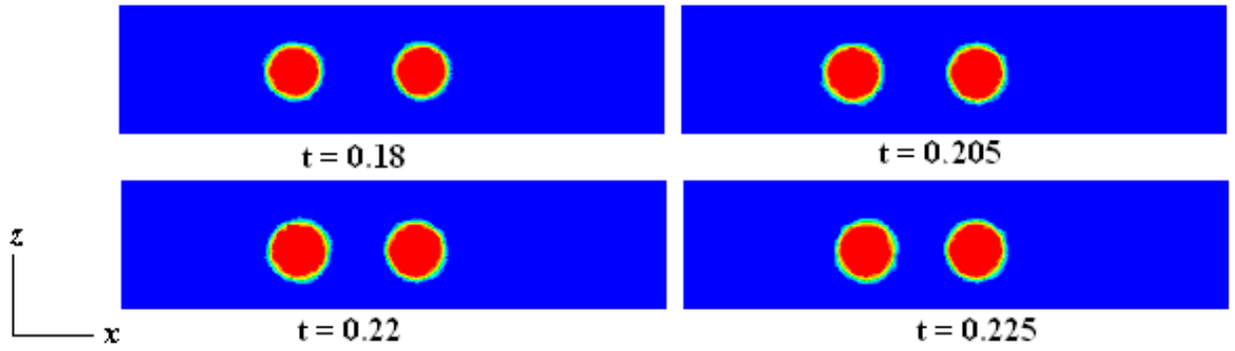

Figure 5. Growth of droplets at horizontal x-z plane at different time level, *We* = 0.0086, *Ca* = 0.0208

With the fixed distance along cross-flow and transverse direction, the maximum porosity of the membrane can be calculated. The porosity is defined as the ratio of the total pore cross-sectional area and the total membrane surface area.

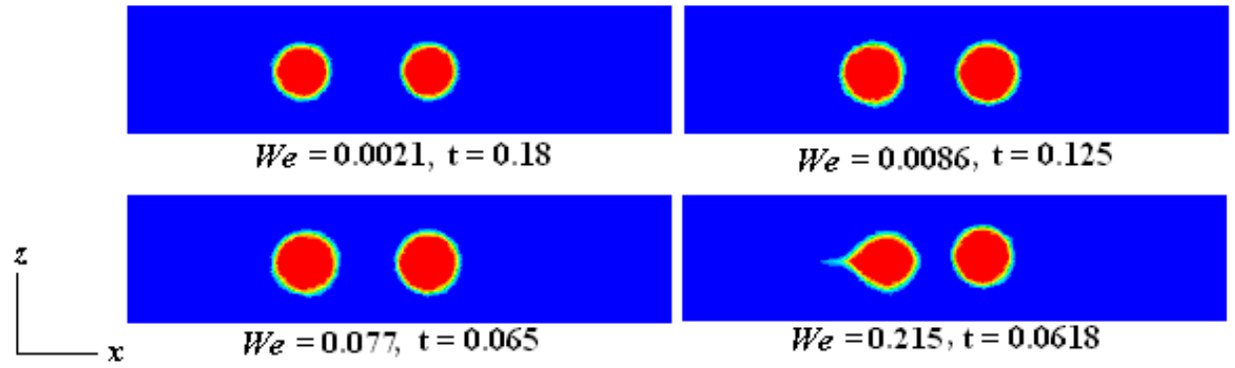

Figure 6. Growth of droplets at horizontal *x*-*z* plane for different values of *We*, *Ca* = 0.0208

To check the effect of *We* on the droplet growth along transverse direction, the simulated results of droplet growth at horizontal plane for different values of *We* and at different time levels have been shown in Fig 6. With the increase in *We* the droplet size increases and the distance between the two droplets decreases along the continuous phase fluid flow direction. At high value of *We* the necking phenomenon has been observed which makes the insufficient distance between the pore for avoiding coalescence. On the other hand at high value of *We* the growth of the droplet in transverse direction is same as the case in lower value of *We*. Thus the spacing of pores in transverse direction can be fixed based on droplet diameter and irrespective of the dripping or jetting mode.

3.2. Effect of dispersed phase flow rate

In order to show the effect of dispersed phase flow rate in droplet dynamics, the droplet growth before the detachment has been shown in Fig.7 for different values of *We* (0.0021

to 0.215) number. The qualitative difference in droplet growth for different values of *We* can be seen in the figure. Some key phenomena such as dripping at low *We* number, necking and jetting at higher *We* number have been observed. During the droplet formation in membrane emulsification process, the inertial force of the dispersed flow acts as detaching force, and acts against the attaching force of surface tension. When inertia force of the dispersed is less than the drag force or interfacial tension force, it cannot influence the droplet dynamics and the droplet growth and detachment are controlled by the drag force competing with the surface tension force. At the low value of *We* (*We* =0.0021) number, the droplet forms and breakups at the micro-pore which is termed as the dripping mode.

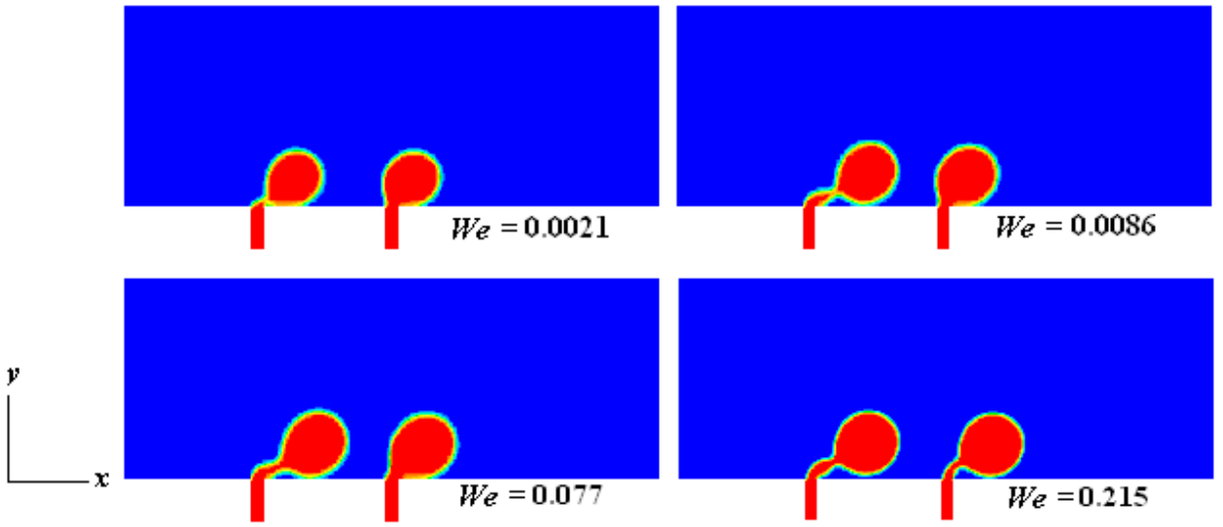

Figure 7. Growth of the droplets for different values of *We*, *Ca* = 0.0208

At intermediate values of Weber number (0.0086 and 0.077), the point of droplet detachment has been moved away from the micro-pore, and formation of dispersed phase thread and necking have been observed. With the increase in inertial force of the dispersed phase, the effective pressure overcomes the capillary pressure inside the liquid thread leading to a stretched filament and also distends the droplet neck noticeably. With the increasing in dispersed phase flow rate further (0.215), two nodes form in the liquid filament and extension of the droplet neck occurs. The detachment point of the droplets moves further downstream from the pore. Thus jetting occurs and the droplet forms at the tip of the droplet. A decrease in the resultant droplet size can be observed. Thus at higher value of *We* number, due to formation of the jetting and the droplet formation from the tip, the distance of 10 pore diameter between the pores is not sufficient to avoid the contact and coalescence of two neighboring droplets.

3.3. Velocity field during droplet growth

The droplet dynamics in membrane emulsification process is controlled by the evolving velocity field outside and inside the dispersed phase since the drag force is correlated to velocity. The velocity fields for *We* = 0.0086 in the central vertical plane (*x*-*y*) at the time level

t = 0.125 have been shown in Fig. 8. Recirculating flows have been observed inside the both droplets and the center of recirculation is different in both the droplets.

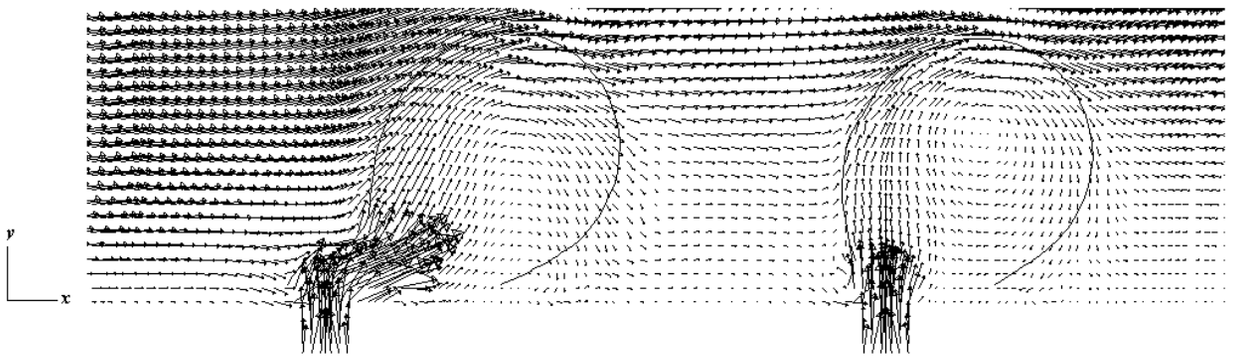

Figure 8. Velocity vector at the central plane, *We* = 0.0086, *Ca* = 0.0208

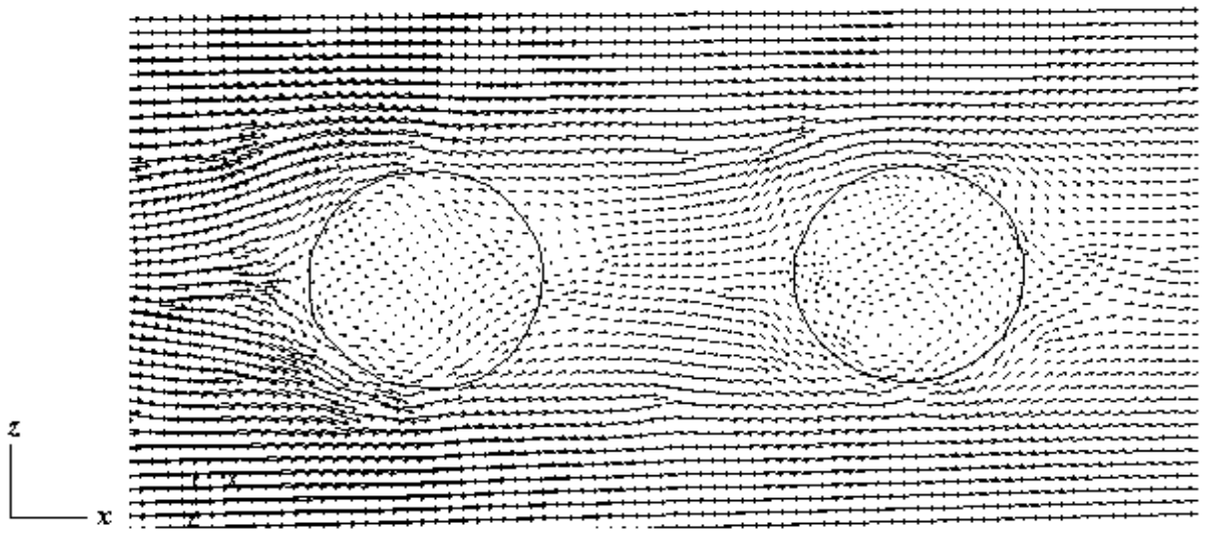

Figure 9. Velocity vector at the horizontal plane, *We* = 0.0086, *Ca* = 0.0208

As the continuous liquid phase interacts the dispersed phase, it imparts a viscous drag force on the evolving interface between the two phases. The viscous drag force produces shear stress along the interface that faces the continuous phase fluid. This initiates the recirculation inside the both droplets. The acceleration of the dispersed phase out of the pore also affects the motion inside the forming drop, especially at an early stage of drop formation. The centre point of the rotational flow inside the drop is at the top of the drop, which is controlled by the above two factors. The dispersed phase inside the interface front finally flows along the continuous liquid phase and is accelerated by the viscous drag. From the velocity diagram it can be seen that the upstream droplet has disturbed the approaching velocity field for the downstream growing droplet. Thus the droplet that grows in the ''shade'' of another droplet experiences a different velocity profile.

The velocity field inside and outside the dispersed phase in horizontal plane (x-z) at the time level (0.125) for *We* = 0.0086 has been shown in Fig. 9. The wake formed by the first droplet is visible from the velocity field, where velocity field is weak.

3.4. Effect of continuous phase velocity

To show the effect of continuous phase velocity, the simulation has been made for same range of Weber number (0.00 to 0.215) but with higher continuous phase flow rate (Q_{cp} = 0.54 l/h). The comparison of droplet diameter for two values of continuous phase velocities i.e. flow rates has been shown in Fig. 10. It has been observed that for the higher continuous phase flow rate, the diameter of the droplets is smaller compared to lower continuous phase flow rate. At a particular value of continuous phase flow rate, the droplet diameter increases with the increase in droplet diameter, than decreases with the increase in droplet diameter due to jetting phenomenon. It can be seen that with the increase in continuous phase velocity, the droplet diameter decreases. Due to increase in velocity, the continuous phase fluid imparts higher drag force and droplet detaches within short interval. It has been also observed that the reduction of droplet diameter during transition from dripping to jetting is less in case of higher value of continuous phase velocity compared to its lower value.

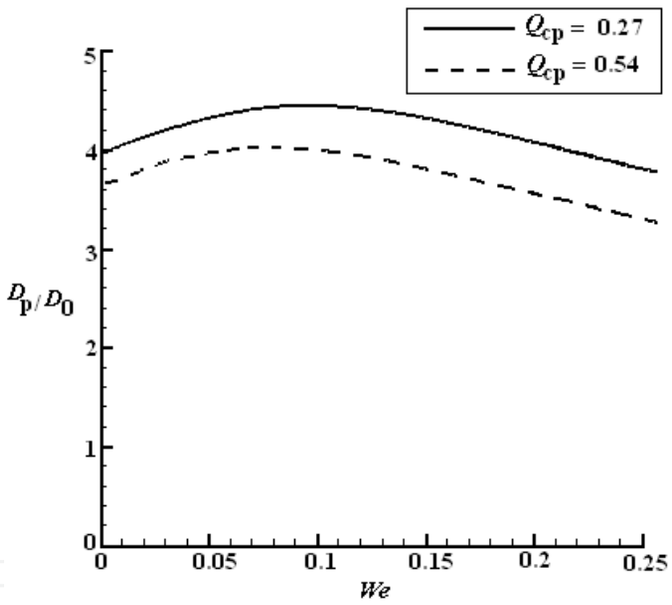

Figure 10. Effect of continuous phase velocity on droplet diameter

The detachment time of droplets for two values of flow rates of continuous phase have been shown in Fig. 11. With lower value of continuous phase flow rate, the detachment time decreases exponentially with the increase in *We* number up to some value of *We* number, after that the decrease rate reduces. At a particular *We* number, the detachment time has been observed less for higher continuous phase flow rate compared to lower continuous phase flow rate. For lower flow rate of continuous phase, the detachment time decreases with the increase of *We* number, but it does not follow the same trend as for the lower flow rate.

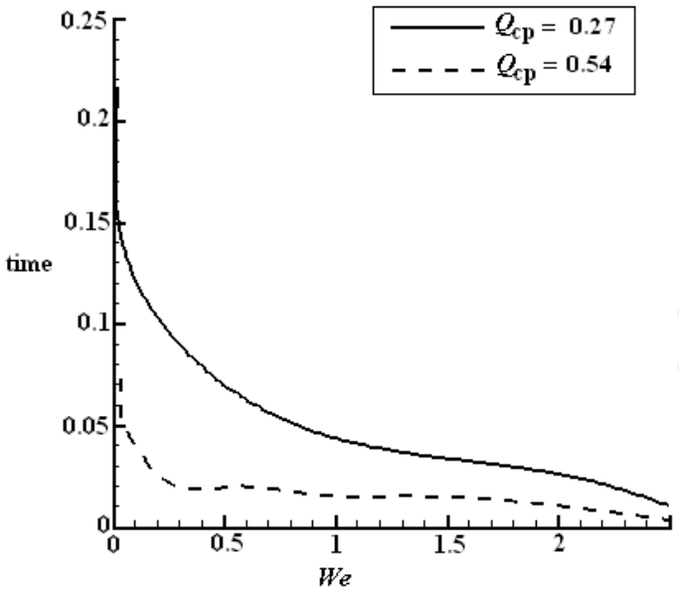

Figure 11. Detachment time of the droplet for different *We* number

3.5. Effect of surface tension

To show the effect of surface tension on the droplet formation, the simulation has been made for different values of surface tension (*Ca* = 0.0208 to 0.0625) at constant value of inertial force. The droplet diameters for different values of *Ca* and two values of continuous phase flow rate have been shown in Fig. 12. With the decrease in surface tension force i.e. increase of *Ca*, the droplet diameter decreases. At low value of surface tension, the attaching surface tension force cannot hold the droplet for longer time against the other detaching forces leading to formation of droplet with smaller size. At very low value of surface tension (0.0008 N/m) even at low value of *We* (0.0021) the phenomenon shows the jetting behavior as shown in Fig. 13. Due to jetting phenomenon, the spacing between the micro-pore is not sufficient to avoid the coalescence of the droplets at two neighbor pores.

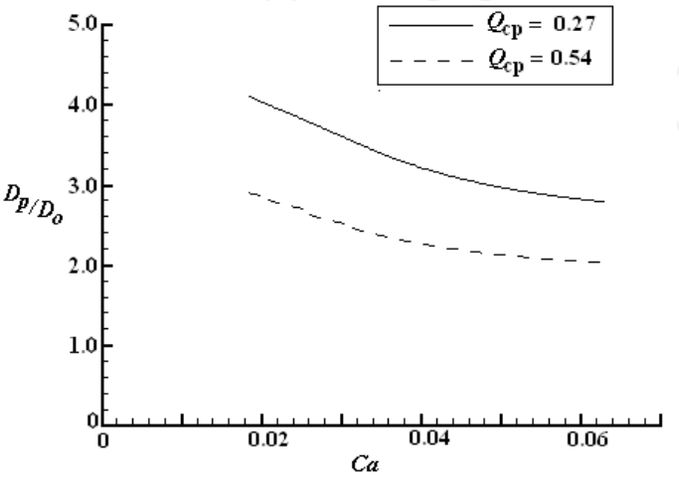

Figure 12. Effect of surface tension on droplet diameter

From the present investigation, it can be seen that dripping to jetting transition can be possible in two ways: one at constant surface tension while varying the inertial force (varying the dispersed phase flow rate) and another at constant inertial force while varying the surface tension force. A qualitative difference in flow pattern in both the transitions has been observed. During dispersed phase controlled transition, the diameter of the drop increases first then decreases rapidly while in surface tension controlled transition, the size of the droplet continuously decreases (Fig. 10 and Fig. 12).

Surface tension force is dominant over the inertial force in dripping mode, hence the droplet size increases and in jetting mode inertial force overcomes the surface tension force for which drop size decreases. In surface controlled breakup, the drag force and interfacial force take part in the droplet formation.

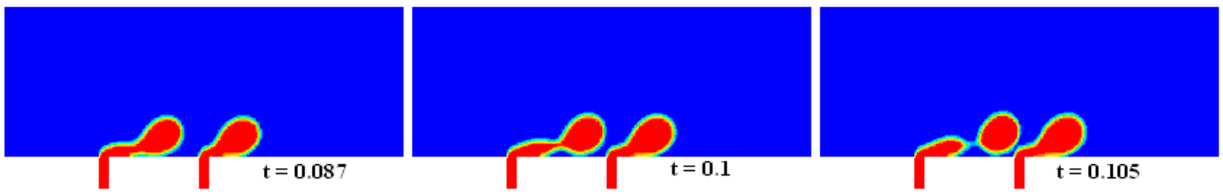

Figure 13. Jetting behavior at low surface tension value

3.6. Effect of viscosities

The viscosities of both the phases also effect the droplet growth and deformation as discussed in introduction section. The drag force which detaches the droplet depends upon the viscosity ratio of dispersed phase and continuous phase. At a constant value of continuous phase flow rate, the drag force increases with the increase in viscosity ratio up to some extent. After that, the drag force becomes independent of the viscosity ratio. Pathak (2011) has observed negligible effect of dispersed phase viscosity in the membrane emulsification system. Moreover it has been also observed that the effect viscosity on droplet dynamics is not very significant if the ratio of dispersed phase and continuous phase viscosity is high (van Dijke et al., 2010). Since the viscosity ratio of dispersed phase and continuous phase fluid is above 3, the effects of viscosities have not been investigated in the present work.

4. Conclusions

Droplet formation in a two-pore membrane emulsification has been numerically investigated in this chapter. The dynamics of droplet formation has been investigated by solving the two-phase governing equations using VOF method. The effects of various parameters, viz., dispersed and continuous phase flow rate, surface tension and viscosities on the droplet dynamics have been investigated. The dynamics of evolution of dispersed phase and droplets formation show the dripping and jetting behavior depending upon the

operating conditions and properties of two-phase liquids in the emulsification system. At constant continuous phase flow rate, the dripping phenomenon occurs at low dispersed phase velocity i.e. at low *We* number and transits towards jetting with the increase in dispersed phase flow rate. At constant continuous phase flow rate, with the increase in dispersed phase flow rate, the droplet size increases initially but decreases as the system transits towards jetting. At constant dispersed phase flow rate, with the increase in continuous phase flow rate, the droplet size decreases and also detachment time. Two ways of dripping to jetting transition have been observed, one with the increasing dispersed phase flow rate at constant continuous phase flow rate and other way is reducing the surface tension at constant dispersed phase flow rate. Both the transitions show different physical structures. The effect of inertia force has been observed the negligible for high value of surface tension and significant for lower surface tension value. The distance between the pore in continuous flow direction depends upon the operating parameters leading to dripping to jetting mode but the pore distance in transverse direction is not affected by the dripping or jetting behavior. Thus at higher value of *We* number, due to formation of the jetting and the droplet formation from the tip, the distance of 10 pore diameter between the pores is not sufficient to avoid the contact and coalescence of two neighboring droplets. The droplet size in the process scales with four main forces: drag forces imparted by the continuous phase, inertia force imparted by dispersed phase, surface tension force and the gravity force. In dripping mode inertial force of dispersed phase has negligible effect as the surface tension and drag force are dominant whereas in jetting mode inertial force of dispersed phase and surface tension force take part in the droplet formation. The evolving vortices are observed in the initial stage of dripping mode but it disappears in later stage. Three important factors must be considered in order to obtain a high production rate in membrane emulsification. (i) A proper combination of continuous phase, dispersed phase flow rate and surface tension so that droplet formation is made just before the starting of surface instability in jetting region. (ii) A proper distribution of pores so that coalescence of droplets does not occur during the droplet growth. (iii) The crossflow velocity must be high enough to provide a sufficient wall shear stress at the membrane surface to transport the drops away from the pore opening and, thus avoid the static hindrance and drop coalescence.

Author details

Manabendra Pathak
Department of Mechanical Engineering, Indian Institute of Technology Patna, India

Nomenclature

A_n	Area of the droplet neck ((μm)^2)
b	Width of the continuous phase channel (μm)
C_a	Capillary number

C_d	Drag coefficient
D_h	Hydraulic diameter of the continuous phase channel (μm)
D_0	Diameter of micro-pore (μm)
D_p	Diameter of the droplet (μm)
f_s	Surface force (N)
F	Volume fraction of dispersed phase fluid
g	Acceleration due to gravity (m/s^2)
h	Height of the continuous phase channel (μm)
k_1	Constant
k_2	Constant
p	Pressure of the flow (Pa)
p_c	Pressure of the continuous phase fluid flow (Pa)
p_d	Pressure of the dispersed phase fluid flow (Pa)
p_γ	Capillary pressure (Pa)
Q_{cp}	Flow rate of continuous phase fluid (m^3/s)
Q_{dp}	Flow rate of dispersed phase fluid (m^3/s)
R	Viscosity ratio of continuous phase to dispersed phase fluid
Re	Reynolds number of the flow
R_p	Reynolds number of the drop
u	Velocity in x- direction (m/s)
u_{cp}	Velocity of continuous phase at the inlet to the channel (m/s)
v	Velocity in y- direction (m/s)
v^*	Local velocity of continuous phase fluid in the channel (m/s)
v_0	Velocity of dispersed phase at the inlet to the micro-pore (m/s)
V	Velocity vector
V_{dr}	Droplet volume((μm)^2)
w	Velocity in z- direction (m/s)
We	Webber number

Greek letters

r	Position vector of interface of the two phase
ϕ	Level set function
κ	Surface curvature (m^{-1})
λ	Viscosity ratio of dispersed phase to continuous phase fluid
μ_{cn}	Viscosity of continuous phase fluid (m^2/s)
μ_{dn}	Viscosity of dispersed phase fluid (m^2/s)
ρ_{cn}	Density of continuous phase fluid (kg/ m^3)
ρ_{dn}	Density of dispersed phase fluid (kg/ m^3)
σ	Surface tension coefficient (N/m)

5. References

Abrahamse, A. J., van der Padt, A. & Boom, R. M. (2002). Analysis of droplet formation and interactions during cross-flow membrane emulsification, J. Membr. Sci. 204: 125-137.

Antanovskii, L. K. (1995) A Phase Field Model of Capillarity. Phys. Fluids 1: 747-753.

Brackbill, J. U., Kith, D. B. & Zemach, C. (1992). A Continuum method for modeling surface tension. J Comp. Phys 100: 335–354.

Churn, I. L., Glimm, J., McBtyan, O., Plohr, B. & Yanic, S. (1986). Front tracking for gas dynamics. J. Comp. Phys. 62: 83-110.

Daly, B. J. (1967). Numerical study of two fluid Rayleigh-Taylor instabilities. Phys. Fluids 10:297-307.

Glimm, J. & McBryan, O. A. (1985). A computational model for interfaces. Adv. Appl. Math. 6: 422-435.

Harlow, F. H. & Welch, J. E. (1966). Numerical study of large-amplitude free-surface motion. Phys. Fluids 9: 842-851.

Hirt, C. W. & Nichols, B. D. (1981). Volume of fluid (VOF) method for the dynamics of free boundaries. J. Comp. Phys. 39: 201-225.

Jacqumin, D. (1996). An energy approach to the continuum surface method. AIAA paper, 96-0858.

Joscelyne, S. M. & Trägårdh, G. (1991). Food emulsions using membrane emulsification: conditions for producing small droplets. J. Food Eng., 39: 59-64.

Joscelyne, S. M. & Trägårdh, G. (2000). Membrane emulsification – a literature review. J. Membr. Sci.169: 107-117.

Karbstein, H., & Schubert, H. (1995). Developments in the continuous mechanical production of oil-in-water macro-emulsions. Chem. Engg. Process. 34: 205-211.

Katoh, R., Asano, Y., Furuya, A., Sotoyama, K. & Tomita, M. (1996). Preparation of food emulsions using membrane emulsification system. J. Membr. Sci. 113: 131-135.

Kobayashi, I., Nakajima, M. & Mukataka, S. (2003). Preparation characteristics of oil-in-water emulsions using differently charged surfactants in straight-through microchannel emulsification. Colloids Surf. A 229: 33–41.

Kobayashi, I., Uemura, K. & Nakajima, M. (2006). CFD study of the effect of a fluid flow in a channel on generation of oil-in-water emulsion droplets in straight-through microchannel emulsification. J. Chem. Eng. Jpn. 39: 855–863.

Luca, G. D., Sindona, A., Giorno, L. & Drioli, E. (2004). Quantitative analysis of coupling effects in cross-flow membrane emulsification. J. Membr. Sci. 229: 199-209.

Nichols, B. D. & Hirt, C. W. (1975). Methods for calculating multi-dimensional, transient free surface flows past bodies. Technical Report LA-UR-75-1932, Los Alamos National Laboratory. NM.

Noh, W. F. & Woodward, P. R. (1976). SLIC (simple line interface methods). In: Voore A I V, P. J. Zandbergen P J, editors. Lecture Notes in Physics 59: 330-340.

Ohta, M., Kikuchi, D., Yoshida, Y. & Sussman, M. (2007). Direct numerical simulation of the slow formation process of single bubbles in a viscous liquid. J. Chem. Eng. Jpn. 40: 939-943.

Osher, S. & Sethian, J. A. (1988). Fronts propagating with curvature-dependent speed: algorithms based on Hamilton-Jacobi formulation. J. Comp. Phys. 79:12-49.

Pathak, M. (2011). Numerical simulation of membrane emulsification: effect of flow properties in the transition from dripping to jetting. J. Membr. Sci. 382: 166-176.

Peng, S., J. & Williams, R. A. (1998). Controlled production of emulsions using a crossflow membrane, Part I: droplet formation from a single pore. Chem. Eng. Res. Des., 76: 894-901.

Rider, W. J. & Kothe, D. B. (1998). Reconstructing volume tracking. J. Comp. Phys 141:112-52.

Rudman, M. (1997). Volume tracking methods for interfacial flow calculations. Int. J. Num. Meth. Fluids. 24: 671-691.

Sang, L., Hong, Y. & Wang, F. (2009). Investigation of viscosity effect on droplet formation in T-shaped microchannels by numerical and analytical methods. Microfluid Nanofluid 6: 621–635.

Schröder, V. & Schubert, H. (1999). Production of emulsions using microporous, ceramic membranes. Colloids Surf A 152: 103-109.

Schubert, H., Ax K, & Behrend, O. (2003). Product engineering of dispersed systems. Trends Food Sci & Technol. 14: 9-16.

Sugiura, S., Nakajima, M., Kumazawa, N., Iwamoto, S. & Seki, M. (2002). Characterization of spontaneous transformation-based droplet formation during microchannel emulsification. J. Phys. Chem. B 106: 9405–9409.

Sussman, M., Smith, K. M., Hussaini, M. Y., Ohta, M. & Zhi-Wei, R. (2007). A sharp interface method for incompressible two-phase flows. J. Comp. Phys. 221: 469-505.

Timgren, A., Trägårdh, G. & Trägårdh. C. (2009). Effects of pore spacing on drop size during cross-flow membrane emulsification—A numerical study. J. Membr. Sci. 337: 232-239.

Tryggvason, G., Bunner, B., Ebrat, O. & Tauber, W. (1998). Computations of multi-phase flow by a finite difference/front tracking method. I. Multi-fluid flows. In Lecture Notes for the 29th Computational Fluid Dynamics Lecture Series, Karman Institute for Fluid Mechanics, Belgium.

van Dijke, K., Kobayashi, I., Schroe¨n, K., Uemura, K., Nakajima, M. & Boom. R. (2010). Effect of viscosities of dispersed and continuous phases in microchannel oil-in-water emulsification, Microfluid Nanofluid. 9**:** 77–85.

Vladisavljevic, G. T. & Schubert, H. (2003). Preparation of emulsions with a narrow particle size distribution using microporous α-alumina membranes. J. Disp. Sci. Technol. 24: 811-819.

Vladisavljevic, G. T., Lambrich, U., Kakajima, M. & Schubert, H. (2004). Production of o/w emulsion using SPG membranes, ceramic α-aluminium oxide membranes, microfluidizer anda silicon microchannel plate - a comparative study. Colloids Surf. A 232: 199-207.

Youngs, D. L. (1982). Time-dependent multi-material flow with large fluid distortion. In: Morton K W, Baines M J, editors, Numerical Methods for Fluid Dynamics, Academic Press 1982.